

# Scattering of massless scalar waves by Reissner-Nordström black holes

Luís C. B. Crispino\*

*Faculdade de Física, Universidade Federal do Pará, 66075-110, Belém, PA, Brazil*

Sam R. Dolan†

*School of Mathematical Sciences, University College Dublin, Belfield, Dublin 4, Ireland*

Ednilton S. Oliveira‡

*Instituto de Física, Universidade de São Paulo, CP 66318, 05315-970, São Paulo, SP, Brazil*

(Dated: November 8, 2018)

We present a study of scattering of massless planar scalar waves by a charged non-rotating black hole. Partial wave methods are applied to compute scattering and absorption cross sections, for a range of incident wavelengths. We compare our numerical results with semi-classical approximations from a geodesic analysis, and find excellent agreement. The glory in the backward direction is studied, and its properties are shown to be related to the properties of the photon orbit. The effects of black hole charge upon scattering and absorption are examined in detail. As the charge of the black hole is increased, we find that the absorption cross section decreases, and the angular width of the interference fringes of the scattering cross section at large angles increases. In particular, the glory spot in the backward direction becomes wider. We interpret these effects under the light of our geodesic analysis.

PACS numbers: 04.40.-b, 04.70.-s, 11.80.-m

## I. INTRODUCTION

Almost a century ago, Schwarzschild discovered a pleasingly simple exact solution to Einstein's gravitational field equations. Ever since, exact solutions have been cherished by theoretical physicists as islands of refuge [1]. That is to say, natural harbors, from which the choppy waters of the non-linear dynamical theory may be safely explored.

Exact black hole solutions are both elegant and simple. Members of the Kerr-Newman family depend on just three numbers: mass  $M$ , charge  $Q$  and angular momentum  $J$  [2]. Uniqueness and stability proofs suggest that these simple stationary spacetimes arise as the generic final outcomes from complicated dynamical processes such as stellar collapse [3].

To examine dynamics, one may try perturbing a black hole away from its stationary configuration. The interaction of fields with Kerr-Newman black holes is of relevance to questions about formation, stability, and gravitational wave emission. For example, it is now well established that *black holes have no hair*; in other words, all long-ranged classical fields ('hair') must decay away [4].

In the 70s and 80s, significant effort was devoted to the study of the scattering and absorption of planar waves that impinge upon black holes in vacuum (cf., e.g., Ref. [5] and references therein). This subject has also received attention in recent years (e.g., see

Refs. [6, 7, 8, 9, 10]). In the standard scenario, authors consider a black hole irradiated by a long-lasting monochromatic plane wave of frequency  $\omega$  which is incident from infinity. Flux is absorbed and scattered, and, if the wave has intrinsic spin, polarized. The resulting scattering pattern may be interpreted as the signature of the black hole. Its features depend primarily upon the dimensionless coupling  $\omega M$ . The large-angle scattering pattern, in particular the so-called *glory* in the backward direction, is inextricably linked to the near-horizon geometry of the hole. It is conceivable that such patterns may one day be observed experimentally at gravitational wave detectors.

Although Reissner-Nordström black holes have not received the same degree of attention as Schwarzschild and Kerr black holes, some effort has been devoted to study the emission and absorption properties of charged black holes. In 1977, Page [11] considered the Hawking emission rates from a nonrotating black hole of small charge, calculated for electrons and muons and their antiparticles. Absorption properties of massive scalars by Reissner-Nordström black holes were analyzed by Jung, Kim, and Park [12]. The absorption and emission spectra of higher-dimensional static charged black holes have been computed by Jung and Park both in the brane and in the bulk for the massless scalar field [13]. The electromagnetic absorption cross section of Reissner-Nordström black holes has been studied by two of the present authors [14]. Notwithstanding, to the best of our knowledge, there are no previous works devoted to planar wave scattering by Reissner-Nordström black holes in the literature. The present paper is dedicated to the study of scattering and absorption of massless scalar waves by static charged black holes in four dimensions.

---

\*Electronic address: [crispino@ufpa.br](mailto:crispino@ufpa.br)

†Electronic address: [sam.dolan@ucd.ie](mailto:sam.dolan@ucd.ie)

‡Electronic address: [ednilton@fma.if.usp.br](mailto:ednilton@fma.if.usp.br)

The Reissner-Nordström spacetime line element is given by

$$ds^2 = f(r)dt^2 - [f(r)]^{-1}dr^2 - r^2 (d\theta^2 + \sin^2\theta d\phi^2), \quad (1)$$

where  $f(r) = (1 - r_+/r)(1 - r_-/r)$  with  $r_{\pm} = M \pm \sqrt{M^2 - Q^2}$ . We use natural units with  $c = G = 1$  and the metric signature  $(+ - - -)$ .

In this work, we exhibit results for three different absolute values of the black hole charge, namely:  $Q = 0$ ,  $|Q| = 0.5M$ , and  $|Q| = M$ . Here,  $Q = 0$  is the Schwarzschild case which was investigated in Refs. [15, 16],  $|Q| = 0.5M$  is a typical Reissner-Nordström black hole example, and  $|Q| = M$  is the extreme Reissner-Nordström black hole case. Our formalism can be used to obtain results for arbitrary values of the ratio  $q \equiv |Q|/M$ , in the interval  $0 \leq q \leq 1$ .

The remainder of the paper is organized as follows: In Sec. II we consider the geodesics of the Reissner-Nordström spacetime. The partial wave approach is outlined in Sec. III, where we give expressions for the massless scalar field, and the absorption and scattering cross sections. Our numerical results are presented in Sec. IV. We conclude with some final remarks in Sec. V.

## II. CLASSICAL ANALYSIS

Here we analyze geodesics in the Reissner-Nordström spacetime. The key results obtained in this section are used to check the validity of our numerical results, obtained from the partial wave scattering analysis of Sec. III.

The geodesics of the Reissner-Nordström spacetime can be found by using Eq. (1) to write

$$\dot{s}^2 = f(r)\dot{t}^2 - [f(r)]^{-1}\dot{r}^2 - r^2 (\dot{\theta}^2 + \dot{\phi}^2 \sin^2\theta) = \kappa, \quad (2)$$

where the “.” denotes the derivative with respect to an affine parameter. For massive particles we have  $\kappa = 1$ , and for massless particles we have  $\kappa = 0$ .

The orbit equation for massless particles is [17]

$$\left(\frac{du}{d\phi}\right)^2 = \frac{1}{b^2} - u^2 + 2Mu^3 - Q^2u^4, \quad (3)$$

where  $u = 1/r$  and  $b$  is the impact parameter. By integrating Eq. (3) we obtain the deflection angle

$$\Theta(b) = \frac{4}{\sqrt{Q^2(u_3 - u_1)(u_2 - u_0)}} [K(k) - F(z, k)] - \pi, \quad (4)$$

where  $F(z, k)$  and  $K(k)$  are the incomplete and complete elliptic integrals of first kind [18], respectively, with

$$k^2 = \frac{(u_3 - u_2)(u_1 - u_0)}{(u_3 - u_1)(u_2 - u_0)},$$

and

$$z = \left[ -\frac{u_0(u_3 - u_1)}{u_3(u_1 - u_0)} \right]^{1/2}.$$

Here,  $u_0, u_1 = 1/r_{\min}$ ,  $u_2$  and  $u_3$  are roots of the right hand side of Eq. (3), and  $r_{\min}$  is the radius of closest approach. For scattering geodesics, the roots obey the inequalities  $u_0 < 0$  and  $u_3 > u_2 \geq u_1 > 0$ . (An analysis of the scattering of null geodesics on the Reissner-Nordström spacetime is presented in Appendix A. A more extensive study of geodesics on black hole spacetimes may be found in [19], for example.)

By differentiating Eq. (3) we get

$$\frac{d^2u}{d\phi^2} + u = 3Mu^2 - 2Q^2u^3. \quad (5)$$

We solved Eqs. (3) and (5) numerically to examine how the black hole charge influences geodesics in Reissner-Nordström spacetime, and compared with the Schwarzschild case. In Fig. 1 we compare the geodesics on different Reissner-Nordström spacetimes. The mass of the hole  $M$  is fixed but the charge-to-mass ratio  $q = |Q|/M$  is varied. We find that, for a fixed impact parameter  $b$ , a larger ratio  $q$  leads to a smaller deflection angle  $\Theta$ .

Using Eqs. (3) and (5) we may derive an analytical approximation to the scattering cross section for small angles. Considering the weak field limit, the deflection angle is found to be [20, 21, 22]:

$$\Theta(b) \approx \frac{4M}{b} + \frac{3\pi}{4} (5 - q^2) \frac{M^2}{b^2}. \quad (6)$$

Note that for large impact parameters we obtain  $\Theta(b) \approx 4M/b$ , which is Einstein's deflection angle [23].

The classical differential scattering cross section is given by

$$\frac{d\sigma_{sc}}{d\Omega} \Big|_{cl} = \frac{b}{\sin\theta} \left| \frac{db}{d\theta} \right|. \quad (7)$$

From Eqs. (6) and (7) we conclude that the classical differential scattering cross section for small angles is

$$\frac{d\sigma_{sc}}{d\Omega} \Big|_{cl} \approx \frac{16M^2}{\theta^4} + \frac{15\pi M^2}{4\theta^3} - \frac{3\pi Q^2}{4\theta^3}. \quad (8)$$

We see that, in the weak field limit, the presence of the black hole charge does not modify the dominant term neither in the deflection angle nor in the scattering cross section. We can thus conclude that in the high-frequency (short-wavelength) limit the differential scattering cross section for small angles must be approximately independent of the black hole charge.

The presence of an unstable photon orbit at  $r = r_c$  (see Appendix A) means that, in theory, geodesics may be deflected through any angle. This property, together with the axial symmetry of our plane-wave scattering scenario,

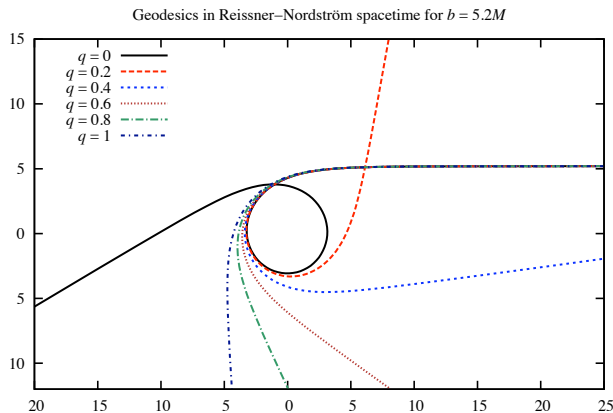


FIG. 1: Geodesics in the Reissner-Nordström spacetime for different values of the ratio  $q = |Q|/M$ . Here, the impact parameter has been chosen to be  $b = 5.2M$ . We see that the black hole has a stronger influence in the particle trajectory for smaller values of  $q$ .

implies that a *glory* will be present. Just as in optics, a glory is a bright spot or halo arising in the scattered intensity in the antipodal direction. The intensity and size of the spot or halo depends on the wavelength of the incident perturbation, leading to chromatic effects. The magnitude and size of the bright spot may be estimated using the approximation derived by Matzner *et al.* [24]

$$\left. \frac{d\sigma_{sc}}{d\Omega} \right|_{\theta \approx \pi} \approx 2\pi\omega b_g^2 \left. \frac{db}{d\theta} \right|_{\theta = \pi} [J_{2s}(\omega b_g \sin \theta)]^2. \quad (9)$$

Here,  $b_g$  is the impact parameter that corresponds to a deflection angle of  $\pi$ ,  $J_{2s}(x)$  is a Bessel function of the first kind (of order  $2s$ ), and  $s$  is the spin of the field ( $s = 0$  for the scalar wave). We recall that Eq. (9) is an approximation valid at high frequencies ( $\omega M \gg 1$ ), for angles close to the backward direction ( $\theta \approx \pi$ ).

The value of  $b_g$  can be obtained (i) by numerically solving the orbit equation (3), or (ii) by considering an analytical approximation of the deflection angle, valid for impact parameters close to the critical one ( $b \approx b_c$ ). We compare the results of methods (i) and (ii) in Appendix A. We find that there is a significant difference between these two approaches. The approximate approach (ii) suggests that the glory peak intensity will decrease monotonically as the black hole charge-to-mass ratio is increased. This is not supported by the numerical approach (i), however. We find that the peak intensity decreases, reaches a minimum, and increases again, as  $q$  increases. This demonstrates that the approximate method (based on the ‘Darwin approximation’ [25]) is not sufficiently accurate for our purposes.

We combined method (i) with the glory approximation (9), to estimate the magnitude and width of the glory. We found

$$\left. \frac{d\sigma_{sc}}{d\Omega} \right|_{\theta \approx \pi} \approx \mathcal{A}(q) [J_0(b_g(q)\omega \sin \theta)]^2, \quad (10)$$

where  $\mathcal{A}(q)/(\omega M^3) = \{30.75, 29.73, 28.87\}$  and  $b_g(q)/M = \{5.36, 5.14, 4.30\}$  for  $q = 0, 0.5, 1$ , respectively. In Sec. IV we check the scattering cross section obtained via the partial wave method against this semi-classical prediction.

### III. PARTIAL WAVE ANALYSIS

#### A. Massless Scalar Field Equation

In curved spacetimes the equation for the minimally-coupled massless scalar field is

$$\nabla^\mu \nabla_\mu \Phi = 0. \quad (11)$$

For  $r > r_+$ , the Reissner-Nordström spacetime, which is spherically symmetric, has a global timelike Killing field,  $\partial_t$ . Hence, we may write

$$\Phi = \frac{\psi_{\omega l}(r)}{r} Y_{lm}(\theta, \phi) e^{-i\omega t}. \quad (12)$$

Here,  $Y_{lm}(\theta, \phi)$  are the scalar spherical harmonics. The radial solutions  $\psi_{\omega l}$  can be expressed in terms of two independent sets of modes: one incoming from the past white-hole horizon  $\mathcal{H}^-$  and other incoming from the past null infinity  $\mathcal{J}^-$  (see, e.g., Ref. [26] for more detail). Here we are dealing with scattering of waves by black holes, so that we need only to consider those modes incoming from  $\mathcal{J}^-$ .

The equation for  $\psi_{\omega l}$  can be written as

$$f(r) \frac{d}{dr} \left[ f(r) \frac{d}{dr} \psi_{\omega l}(r) \right] + [\omega^2 - V_{eff}(r)] \psi_{\omega l}(r) = 0, \quad (13)$$

where the effective potential is given by

$$V_{eff}(r) = f(r) \left[ \frac{1}{r} \frac{df(r)}{dr} + \frac{l(l+1)}{r^2} \right]. \quad (14)$$

To better treat the solution of Eq. (13) in the asymptotic limits, we introduce the tortoise coordinate  $x$  defined by

$$\frac{d}{dx} = f(r) \frac{d}{dr}, \quad (15)$$

or, in integral form,

$$x = r + \frac{r_+^2}{r_+ - r_-} \ln \left| \frac{r}{r_+} - 1 \right| - \frac{r_-^2}{r_+ - r_-} \ln \left| \frac{r}{r_-} - 1 \right| + C, \quad (16)$$

where  $C$  is an integration constant. Our numerical results for the scattering cross section are independent of the choice of  $C$ , and we have set  $C = 0$ .

In terms of the tortoise coordinate, the radial equation (13) may be written as

$$\frac{d^2}{dx^2} \psi_{\omega l}(x) + [\omega^2 - V_{eff}(x)] \psi_{\omega l}(x) = 0. \quad (17)$$

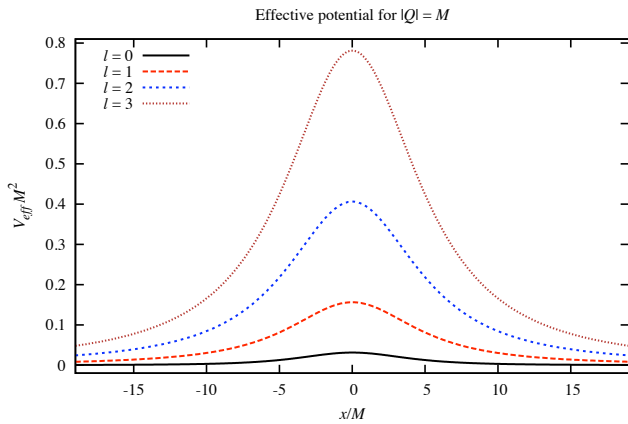


FIG. 2: The effective potential for the extreme Reissner-Nordström black hole as a function of the tortoise coordinate (16), plotted for different choices of  $l$ .

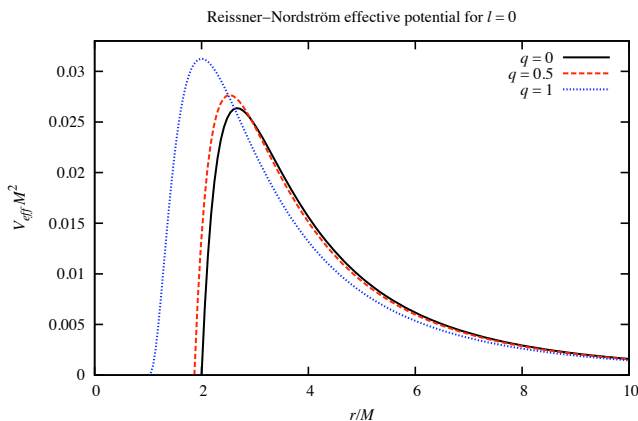


FIG. 3: The effective potential given by Eq. (14) with  $l = 0$  is plotted for  $q = 0$  (solid line),  $q = 0.5$  (dashed line), and  $q = 1$  (dotted line). The effective potential goes to zero at the event horizon and at infinity. As we can see, the maximum of the potential increases as the black hole charge increases.

In Fig. 2 we plot the effective potential as a function of the tortoise coordinate for an extreme Reissner-Nordström black hole.

In Fig. 3 we compare the effective potential, with  $l = 0$ , for the three cases:  $Q = 0$ ,  $|Q| = 0.5M$ , and  $|Q| = M$ . As we can see, the effective potential goes to zero as  $r \rightarrow r_+$  and as  $r \rightarrow \infty$ , for all cases. The height of the effective potential barrier increases with the charge-to-mass ratio  $q$ .

For  $r \gg r_+$ , we have

$$\psi_{\omega l}(x) \approx \omega x \left[ (-i)^{l+1} A_{\omega l}^{in} h_l^{(1)*}(\omega x) + i^{l+1} A_{\omega l}^{out} h_l^{(1)}(\omega x) \right], \quad (18)$$

where  $h_l^{(1)}(x)$  are the spherical Bessel functions of the third kind [18], and  $A_{\omega l}^{in}$  and  $A_{\omega l}^{out}$  are complex constants.

Now, recalling that  $h_l^{(1)}(x) \approx (-i)^{l+1} e^{ix}/x$  as  $x \rightarrow \infty$ , and using that the effective potential goes to zero as  $x \rightarrow$

$-\infty$ , we get

$$\psi_{\omega l}(x) \approx \begin{cases} A_{\omega l}^{tr} e^{-i\omega x} & (x \rightarrow -\infty), \\ A_{\omega l}^{in} e^{-i\omega x} + A_{\omega l}^{out} e^{i\omega x} & (x \rightarrow \infty), \end{cases} \quad (19)$$

with the relation  $|A_{\omega l}^{in}|^2 = |A_{\omega l}^{out}|^2 + |A_{\omega l}^{tr}|^2$  satisfied.

## B. Absorption Cross Section

The total absorption cross section can be written as

$$\sigma_{abs} = \sum_{l=0}^{\infty} \sigma_{abs}^{(l)}, \quad (20)$$

where  $\sigma_{abs}^{(l)}$  is the partial absorption cross section, namely

$$\sigma_{abs}^{(l)} = \frac{\pi}{\omega^2} (2l+1) \left( 1 - \left| \frac{A_{\omega l}^{out}}{A_{\omega l}^{in}} \right|^2 \right). \quad (21)$$

From the classical analysis, developed in Sec. II, the geometrical optics (high-frequency) limit of the total absorption cross section can be found to be

$$\sigma_{abs}^{hf} = \pi \frac{(3M + \sqrt{9M^2 - 8Q^2})^4}{8(3M^2 - 2Q^2 + M\sqrt{9M^2 - 8Q^2})}. \quad (22)$$

It is easy to check that for  $Q = 0$  we get from Eq. (22)  $\sigma_{abs}^{hf} = 27\pi M^2 = (27/4)\pi r_+^2$  [27]. (We recall that  $r_+ = 2M$  and  $r_- = 0$  in the Schwarzschild case.) For  $|Q| = M$  we get  $\sigma_{abs}^{hf} = 16\pi M^2 = 16\pi r_+^2$ . (We recall that  $r_+ = r_- = M$  in the extreme Reissner-Nordström case.)

## C. Scattering Cross Section

The phase shifts of the scattered waves are defined by

$$\exp[2i\delta_l(\omega)] = (-1)^{l+1} \frac{A_{\omega l}^{out}}{A_{\omega l}^{in}}. \quad (23)$$

The scattering amplitude is given by

$$g(\theta) = \frac{1}{2i\omega} \sum_{l=0}^{\infty} (2l+1) \left[ e^{2i\delta_l(\omega)} - 1 \right] P_l(\cos\theta), \quad (24)$$

and the differential scattering cross section is

$$\frac{d\sigma_{sc}}{d\Omega} = |g(\theta)|^2. \quad (25)$$

A selection of our key results for the absorption and scattering cross sections is presented in the next section. The numerical method we have used is described in Ref. [28]. In addition, we have used the method developed in Refs. [7, 29] to improve the numerical convergence of the partial wave series (24).

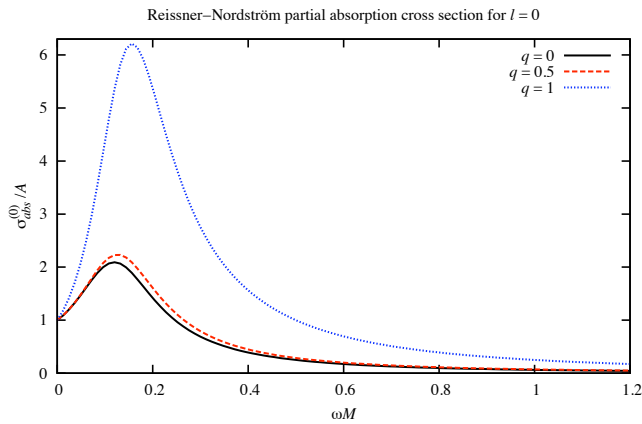


FIG. 4: The partial absorption cross section with  $l = 0$  plotted for Reissner-Nordström black holes, with  $q = 0$  (solid line),  $q = 0.5$  (dashed line), and  $q = 1$  (dotted line). We see that  $\sigma_{abs}^{(0)} \rightarrow A$  as  $\omega M \rightarrow 0$ .

#### IV. RESULTS

In Fig. 4 we plot the partial absorption cross section of Reissner-Nordström black holes divided by the black hole area,  $A = 4\pi r_+^2$ , for  $l = 0$ , and for  $q = 0$  (Schwarzschild case),  $q = 0.5$  (typical Reissner-Nordström case) and  $q = 1$  (extreme case). We see that in the low-frequency limit we have  $\sigma_{abs}^{(0)lf} = A$  [30, 31]. In this limit, the only nonvanishing contribution to the total absorption cross section comes from the isotropic mode with  $l = 0$ .

The total absorption cross section of Reissner-Nordström black holes is plotted in Fig. 5, for the same three choices of the charge ( $q = 0, 0.5, 1$ ). As we can see, the absorption cross section decreases as the charge-to-mass ratio increases. (The same behavior is observed for the electromagnetic field absorption cross section [14].) This is in concordance with the observation that the height of the effective potential barrier (see Fig. 3) increases with the charge-to-mass ratio. The straight lines in Fig. 5 show the geometric-optics limit for each case.

In Fig. 6 we plot the differential scattering cross sections of Reissner-Nordström black holes for the massless scalar field at  $\omega M = 3.0$ . The values chosen for the black hole charge are again such that  $q = 0, q = 0.5$  and  $q = 1$ . In this figure we also plot the glory scattering cross sections given in Eq. (10). We find an excellent agreement between the numerical results and the glory approximation for  $\theta \approx \pi$ .

We compare the scattering cross sections in Fig. 7, for the same choices of the black hole charge ( $q = 0, 0.5, 1$ ), at  $\omega M = 1.0$ . In Fig. 8 we make the same comparison for  $\omega M = 3.0$ . We see that, at fixed frequency, the glory peak is wider for larger values of the charge-to-mass ratio  $q$ . This can be understood by the fact that, from Eq. (9), the glory peak width is proportional to  $1/(b_g\omega)$ , and from Eq. (10) we see that  $b_g$  is smaller for larger values of  $q$ .

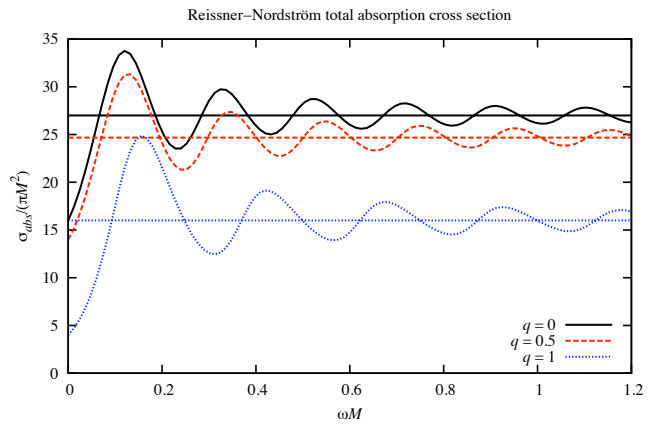


FIG. 5: Reissner-Nordström absorption cross section for  $q = 0, q = 0.5$ , and  $q = 1$ . We see that the total absorption cross section decreases as the black hole charge increases.

#### V. FINAL REMARKS

In the preceding sections, we have computed absorption and scattering cross sections for planar monochromatic massless scalar waves impinging upon Reissner-Nordström black holes. We found that the interaction depends on frequency  $\omega M$  and charge-to-mass ratio  $q = |Q|/M$ . We developed the formalism needed to obtain scattering and absorption cross sections for arbitrary values of  $0 \leq q \leq 1$ . We showed typical results for three different values of the charge-to-mass ratio of the black hole, namely:  $q = 0, q = 0.5$ , and  $q = 1$ .

What, then, are the effects of black hole charge upon the scattering and absorption of massless scalar waves? Let us summarize. The effect on absorption is clear: the absorption cross section decreases as the charge-to-mass ratio increases (Fig. 5). This is compatible with the fact that the horizon area shrinks from  $16\pi M^2$  at  $q = 0$  to  $4\pi M^2$  at  $q = 1$ . In our numerical results we have observed that, in the low-frequency limit, the absorption cross section tends to the black hole area (Fig. 4) [30]. This is a general result for the absorption cross section of the minimally-coupled massless scalar field in stationary black hole spacetimes [31]. We have also observed that, in the high-frequency limit, the absorption cross sections oscillates about the geometric-optics value (Fig. 5). Similar behavior has previously been observed for the electromagnetic field [14].

The effects of black hole charge upon wave scattering are more subtle. By using the weak-field approximation (6), we showed that the scattering cross section at small angles ( $\theta \approx 0$ ) is still dominated by the “Schwarzschild term”  $16M^2/\theta^4$  [cf. Eq. (8)]. Black hole charge leads only to a subdominant correction term proportional to  $Q^2/\theta^3$  at small angles. However, the black hole charge does have a significant effect upon the cross section observed at large angles (Figs. 7 and 8). We found that the angular width of the so-called spiral scattering os-

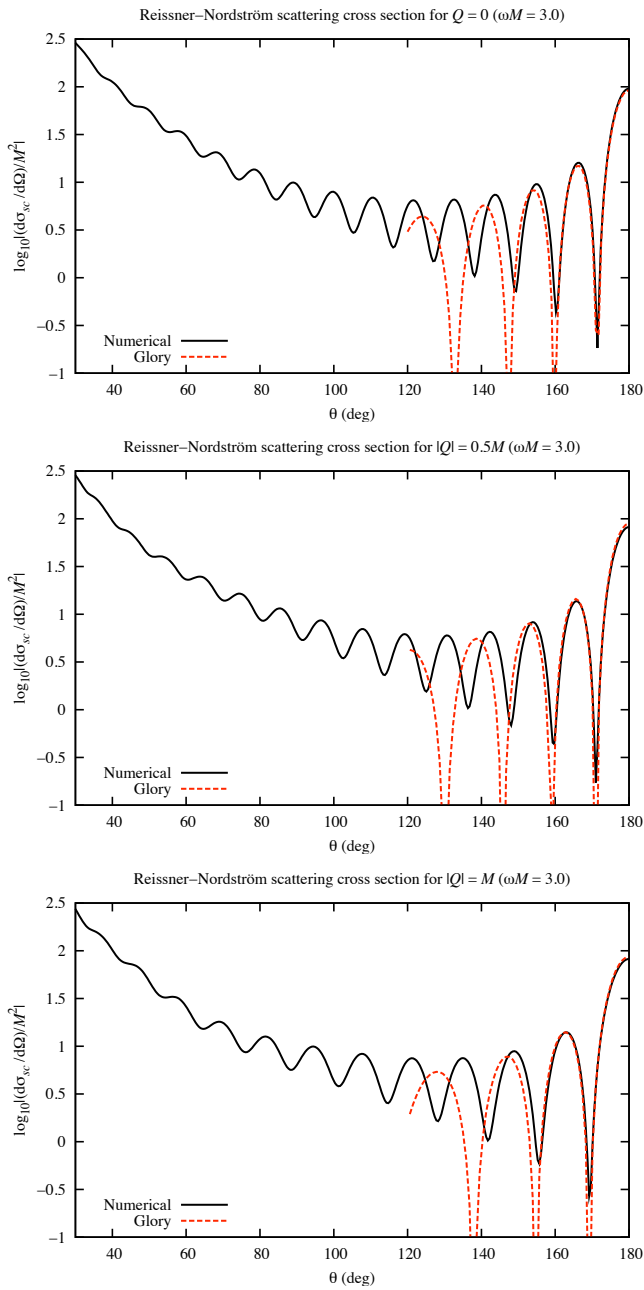


FIG. 6: Comparison between the scattering cross section of Reissner-Nordström black holes and the glory approximation at  $\omega M = 3$ , for  $q = 0, 0.5, 1$ . As we can see, for the three cases, the numerical results are in excellent agreement with the glory approximation for angles close to  $180^\circ$ .

cillations increases with  $q$ . In particular, the glory peak becomes wider as  $q$  increases (Fig. 6). These effects are related to the fact that the radius of the photon orbit shrinks as  $q$  increases.

In principle, highly accurate measurements of, for example, the gravitational wave flux scattered by a black hole could one day be used to estimate black hole's charge. A more immediate possibility is that scattering

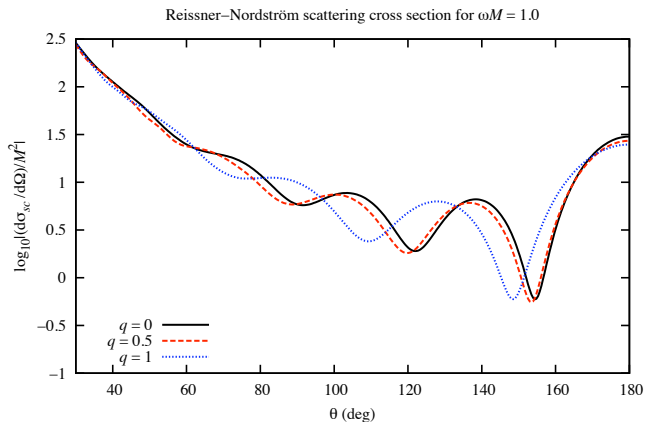


FIG. 7: Scattering cross section for Reissner-Nordström black holes with charges  $q = 0$  (solid line),  $q = 0.5$  (dashed line), and  $q = 1$  (dotted line), for  $\omega M = 1.0$ . The width of the glory peak gets wider for bigger values of the black hole charge.

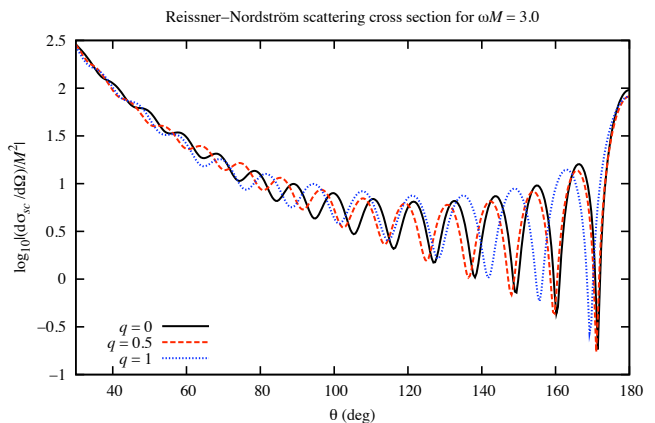


FIG. 8: Scattering cross section for Reissner-Nordström black holes with charges  $q = 0$ ,  $q = 0.5$  and  $q = 1$ , for  $\omega M = 3.0$ . Here, as in Fig. 7, the width of the glory peak increases as the black hole charge increases.

and absorption patterns may be observed with black hole analogue systems created in the laboratory [28]. Even if experimental verification is not forthcoming, we hope that studies of wave scattering by black holes will continue to improve our understanding of how black holes interact with their environments.

### Acknowledgments

The authors would like to thank Conselho Nacional de Desenvolvimento Científico e Tecnológico (CNPq) for partial financial support. S. D. acknowledges financial support from the Irish Research Council for Science, Engineering and Technology (IRCSET). S. D. and E. O. thank the Universidade Federal do Pará (UFPA) in Belém for kind hospitality. L. C. and E. O. would like

to acknowledge also partial financial support from Coordenação de Aperfeiçoamento de Pessoal de Nível Superior (CAPES).

## APPENDIX A: ANALYTICAL APPROXIMATION FOR THE GLORY COEFFICIENTS

Here we derive an approximation to the deflection angle given in Eq. (4), in order to obtain an analytic expression for the glory impact parameter  $b_g$  and its derivative. Our aim is to estimate the magnitude and width of the glory peak for Reissner-Nordström black hole scattering. Let us begin by finding the roots of the right hand side of Eq. (3) when the impact parameter is critical ( $b = b_c$ ). We have

$$\bar{u}_0 = \left[ (M + y) - 2\sqrt{M(M + y)} \right] / 4Q^2, \quad (\text{A1})$$

$$\bar{u}_1 = u_c = (3M - y) / 4Q^2, \quad (\text{A2})$$

$$\bar{u}_2 = u_c, \quad (\text{A3})$$

$$\bar{u}_3 = \left[ (M + y) + 2\sqrt{M(M + y)} \right] / 4Q^2, \quad (\text{A4})$$

where  $y = \sqrt{9M^2 - 8Q^2}$ . Note that a root is repeated in the critical case:  $u_1 = u_2 = u_c$ . The radius of the circular photon orbit is  $r_c = 1/u_c$ . The critical impact parameter is

$$b_c = \frac{(3M + y)^2}{\sqrt{8(3M^2 - 2Q^2 + My)}}. \quad (\text{A5})$$

In the Schwarzschild limit ( $Q = 0$ ) we recover  $u_0 = -1/6M$ ,  $u_1 = u_2 = 1/3M$ ,  $u_3 = +\infty$  and  $b_c = \sqrt{27}M$  [23].

When the impact parameter is close to critical ( $b \approx b_c$ ), the perturbed roots are

$$u_0 = \bar{u}_0 + \mathcal{O}(\delta^2), \quad (\text{A6})$$

$$u_1 = u_c - u_c \delta \Delta + \mathcal{O}(\delta^2), \quad (\text{A7})$$

$$u_2 = u_c + u_c \delta \Delta + \mathcal{O}(\delta^2), \quad (\text{A8})$$

$$u_3 = \bar{u}_3 + \mathcal{O}(\delta^2), \quad (\text{A9})$$

where  $\delta^2 = (b - b_c)/b_c$  and  $\Delta^2 = 2/(6 - u_c^2 b_c^2)$ .

For near-critical orbits we find that the coefficient  $k$  of the elliptic integrals in Eq. (4) behaves as

$$k^2 = 1 - \frac{2u_c(\bar{u}_3 - \bar{u}_0)\Delta}{(\bar{u}_3 - u_c)(u_c - \bar{u}_0)}\delta + \mathcal{O}(\delta^2). \quad (\text{A10})$$

To derive the logarithmic deflection formula, we make use of the approximations for  $k \approx 1$

$$K(k) \approx \frac{1}{2} \ln \left( \frac{16}{1 - k^2} \right), \quad (\text{A11})$$

$$F(z, k) \approx \frac{1}{2} \ln \left( \frac{1 + z}{1 - z} \right), \quad (\text{A12})$$

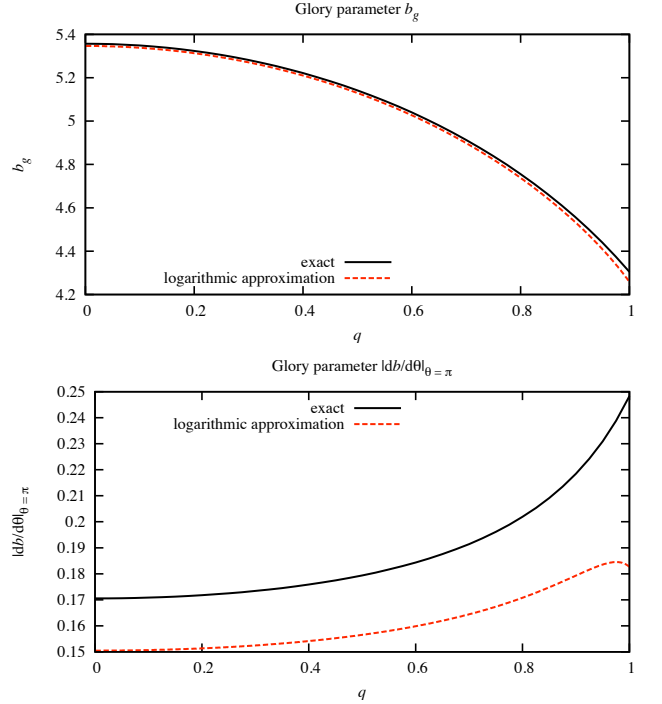


FIG. 9: Glory parameters  $b_g$  and  $|db/d\theta|_{\theta=\pi}$  shown as a function of  $q$ . The plots compare the approximation Eq. (A13) (dotted line) with accurate results from numerical integration (solid line). The approximation for  $|db/d\theta|_{\theta=\pi}$  is clearly less good than the approximation of  $b_g$ , and the accuracy diminishes further as  $q \rightarrow 1$ .

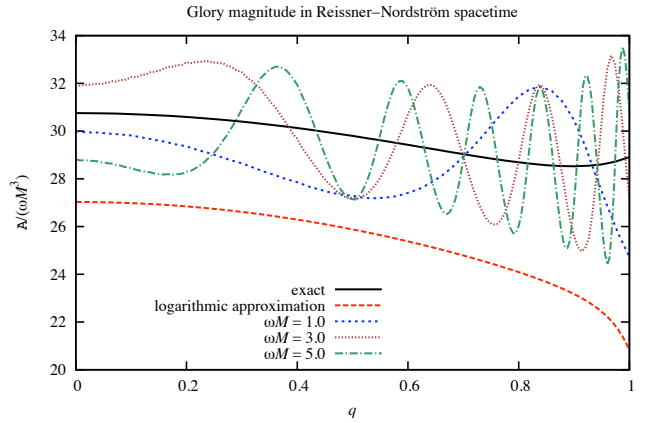


FIG. 10: Intensity of the glory peak  $\mathcal{A}$  as a function of  $q$ . The prediction of the logarithmic approximation is compared with the exact solution of the orbital equation. We also show the intensity of the glory peak computed numerically via the partial wave method for  $\omega M = 1.0, 3.0, \text{ and } 5.0$ .

and also  $(u_3 - u_c)(u_c - u_0) = 2/(Qu_c b_c \Delta)^2$  and  $u_3 - u_0 = M\sqrt{1 + y/M}/Q^2$ . Putting all these elements into Eq. (4), we find

$$\Theta(b) \approx -\alpha(q) \ln \left( \frac{b - b_c}{\beta(q)M} \right), \quad (\text{A13})$$

where the dimensionless coefficients are

$$\alpha(q) = \frac{u_c b_c}{\sqrt{6 - u_c^2 b_c^2}}, \quad (\text{A14})$$

$$\beta(q) = \frac{32(6 - u_c^2 b_c^2)^3}{u_c^6 b_c^3 M^3 (1 + y/M)} \frac{(1 - z)^2}{(1 + z)^2} e^{-\pi/\alpha(q)}. \quad (\text{A15})$$

The glory formula is

$$\frac{d\sigma_{sc}}{d\Omega} \Big|_{\theta \approx \pi} \approx \mathcal{A}(q) [J_{2s}(b_g \omega \sin \theta)]^2, \quad (\text{A16})$$

where the magnitude of the glory peak is given by

$$\mathcal{A}(q) = 2\pi\omega b_g^2 \left| \frac{db}{d\theta} \right|_{\theta=\pi}. \quad (\text{A17})$$

In Fig. 9 we compare the values of  $b_g$  and  $|db/d\theta|_{\theta=\pi}$  calculated from approximation (A13) with exact values determined from numerical integration. It shows clearly that the estimate of  $b_g$  found from (A13) is significantly more accurate than the corresponding estimate of its derivative with respect to  $\theta$ .

The magnitude of the glory peak obtained using the logarithmic approximation [Eqs. (A13)–(A15) and (A17)] is plotted in Fig. 10, and it can be seen that it decreases with  $q$ . The logarithmic scattering results suggest that the glory magnitude for  $q = 1$  should be significantly smaller than for  $q = 0$ . In Fig. 10 we also show the values of  $\mathcal{A}(q)$  obtained by solving the orbital equation (3)

numerically. It is interesting that these two approaches disagree significantly near  $q = 1$  (the curve obtained using the orbital equation goes up whereas the logarithmic approximation curve goes down). It is clear that the exact solution does not agree with the logarithmic approximation for the glory scattering. For instance, for the Schwarzschild case, the logarithmic approximation gives [25]  $\mathcal{A}(q = 0) = 27.029\omega M^3$  whereas the exact value is  $\mathcal{A}(q = 0) = 30.752\omega M^3$ . We find  $b_g = 5.346635M$  and  $|db/d\theta|_{\theta=\pi} = 0.150483M$  for the logarithmic approximation, compared with  $b_g = 5.356959M$  and  $|db/d\theta|_{\theta=\pi} = 0.170554M$ , obtained numerically. As we can see from Fig. 9, most of the error in the logarithmic approximation comes from the derivative of  $b$  with respect to  $\theta$ . The values of  $\mathcal{A}(q)$  obtained via the partial wave method (cf. Sec. III C) for  $\omega M = 1.0, 3.0$ , and  $5.0$  are also shown in Fig. 10. We see that they oscillate around the semiclassical result obtained using the orbital equation (3).

Finally we note that the glory approximation (9) may be improved by including the contribution from geodesics passing more than once around the black hole (i.e. through angles  $3\pi, 5\pi$ , etc.) [5]. Higher-order contributions of this kind will be suppressed by successive factors of  $e^{-2\pi/\alpha(q)}$ . Since the largest value of  $\alpha(q)$  is  $\alpha(1) \approx 1.4142$ , subsequent contributions will be suppressed by at least  $e^{-2\pi/1.4142} \approx 1.2 \times 10^{-2}$ . We neglect these contributions here, although elsewhere it was shown [10] that adding the second-order contribution may improve the approximation slightly.

- 
- [1] H. Stephani, D. Kramer, M. A. H. MacCallum, C. Hoenselaers, and E. Herlt, *Exact Solutions of Einstein's Field Equations* (Cambridge University Press, Cambridge, England, 2003), 2nd ed.
- [2] C. W. Misner, K. S. Thorne, and J. A. Wheeler, *Gravitation* (Freeman, San Francisco, 1973).
- [3] S. W. Hawking and G. F. R. Ellis, *The Large Scale Structure of Space-Time* (Cambridge University Press, Cambridge, England, 1973).
- [4] V. P. Frolov and I. D. Novikov, *Black Hole Physics: Basic Concepts and New Developments* (Kluwer Academic Publishers, Dordrecht, The Netherlands, 1998).
- [5] J. A. H. Futterman, F. A. Handler, and R. A. Matzner, *Scattering from Black Holes* (Cambridge University Press, Cambridge, England, 1988).
- [6] K. Glampedakis and N. Andersson, *Class. Quantum Grav.* **18**, 1939 (2001).
- [7] C. Doran, A. Lasenby, S. Dolan, and I. Hinder, *Phys. Rev. D* **71**, 124020 (2005).
- [8] S. R. Dolan, C. J. L. Doran, and A. N. Lasenby, *Phys. Rev. D* **74**, 064005 (2006).
- [9] L. C. B. Crispino, E. S. Oliveira, A. Higuchi, and G. E. A. Matsas, *Phys. Rev. D* **75**, 104012 (2007).
- [10] S. R. Dolan, *Class. Quantum Grav.* **25**, 235002 (2008).
- [11] D. N. Page, *Phys. Rev. D* **16**, 2402 (1977).
- [12] E. Jung, S. H. Kim, and D. K. Park, *Phys. Lett. B* **602**, 105 (2004).
- [13] E. Jung and D. K. Park, *Nucl. Phys. B* **717**, 272 (2005).
- [14] L. C. B. Crispino and E. S. Oliveira, *Phys. Rev. D* **78**, 024011 (2008).
- [15] N. G. Sánchez, *J. Math. Phys. (N.Y.)* **17**, 688 (1976); *Phys. Rev. D* **16**, 937 (1977); **18**, 1030 (1978); **18**, 1798 (1978).
- [16] N. Andersson, *Phys. Rev. D* **52**, 1808 (1995).
- [17] S. Chandrasekhar, *The Mathematical Theory of Black Holes* (Oxford University Press, New York, 1983).
- [18] M. Abramowitz and I. A. Stegun, *Handbook of Mathematical Functions* (Dover Publications, New York, New York, 1965).
- [19] G. Slezáková, *Geodesic Geometry of Black Holes*, Ph.D. thesis, University of Waikato, New Zealand, 2006. Available at <http://adt.waikato.ac.nz/public/adt-uow20061024.003016/index.html>.
- [20] E. F. Eiroa, G. E. Romero, and D. F. Torres, *Phys. Rev. D* **66**, 024010 (2002).
- [21] A. Bhadra, *Phys. Rev. D* **67**, 103009 (2003).
- [22] M. Sereno, *Phys. Rev. D* **69**, 023002 (2004).
- [23] R. M. Wald, *General Relativity* (The University of Chicago Press, Chicago, Illinois, 1984).
- [24] R. A. Matzner, C. DeWitt-Morette, B. Nelson, and T.-R. Zhang, *Phys. Rev. D* **31**, 1869 (1985).
- [25] C. Darwin, *Proc. R. Soc. A* **249**, 180 (1959).
- [26] L. C. B. Crispino, A. R. R. da Silva, and G. E. A. Matsas, *Phys. Rev. D* **79**, 024004 (2009).

- [27] B. Mashhoon, Phys. Rev. D **7**, 2807 (1973).
- [28] S. R. Dolan, E. S. Oliveira, and L. C. B. Crispino, *Scattering of Sound Waves by a Canonical Acoustic Hole*, accepted for publication in Phys. Rev. D (expected to be published in the March 2009 issue). L. C. B. Crispino, E. S. Oliveira, and G. E. A. Matsas, Phys. Rev. D **76**, 107502 (2007).
- [29] D. R. Yennie, D. G. Ravenhall, and R. N. Wilson, Phys. Rev. **95**, 500 (1954).
- [30] S. R. Das, G. Gibbons, and S. D. Mathur, Phys. Rev. Lett. **78**, 417 (1997).
- [31] A. Higuchi, Class. Quantum Grav. **18**, L139 (2001); **19**, 599 (2002).